IEEE Access
Multidisciplinary ⋮ Rapid Review ⋮ Open Access Journal

Received 12 August 2024, accepted 4 September 2024, date of publication 9 September 2024,
date of current version 19 September 2024.

Digital Object Identifier 10.1109/ACCESS.2024.3456087

RESEARCH ARTICLE

A Novel Frequency Reference Compensation Method in Decentralized Secondary Frequency Control for Parallel Operation of Multiple Generators in an Islanded Microgrid

JUN-HYEOK KIM[1], (Student Member, IEEE), JAE-WON CHANG[2], (Member, IEEE), AND YUN-SU KIM[1], (Senior Member, IEEE)

[1]Graduate School of Energy Convergence, Gwangju Institute of Science and Technology, Gwangju 61005, South Korea
[2]School of Energy Systems Engineering, Chung-Ang University, Seoul 06974, South Korea

Corresponding author: Yun-Su Kim (yunsukim@gist.ac.kr)

This work was supported by Korea Institute of Energy Technology Evaluation and Planning (KETEP) and the Ministry of Trade, Industry and Energy (MOTIE) of Republic of Korea under Grant 20204010600340.

ABSTRACT Conventional centralized and distributed structures for secondary frequency control (SFC) in an islanded microgrid rely on communications. However, this may degrade the reliability of the system if communication delays or failures occur. As a potential alternative, several decentralized integral controls have emerged for SFC of islanded microgrids; however, these methods are limited by their inability to account for the unknown biased errors of real systems, which can accumulate in the controller of each generator causing clock drift and fighting among the generators. To overcome these issues, this paper proposes a novel SFC method for diesel generators in an islanded microgrid. With the proposed method, the frequency can be maintained at almost the nominal value by "frequency reference compensation control (FRCC)" with only local measurements that do not require telecommunications. Therefore, this approach prevents catastrophic circumstances due to communication failures and delays in islanded microgrids. The proposed controller has improved robustness against unknown biased errors, thus mitigating fighting among multiple diesel generators. To ensure system stability, small-signal stability analyses and common quadratic Lyapunov method were conducted with switched state-space modeling. The small-signal stability analyses show that the proposed method shifts the unstable eigenvalue at the critical point of the system matrix to the negative real part, ensuring the system is asymptotically stable. Control parameters are achieved via heuristic optimization called particle swarm optimization (PSO). Hardware in the loop simulations were performed to verify the feasibility of the proposed control method.

INDEX TERMS Clock drift, decentralized control, islanded microgrids, secondary frequency control, switched state-space modeling.

I. INTRODUCTION

Power systems require stable and reliable frequency control for optimal operation. Especially in an islanded microgrid, where the system frequency relies on a few diesel generators with low inertia, the frequency can fluctuate significantly and more frequently compared to conventional power systems. Furthermore, increasing the integration of renewable generators magnifies the seriousness of these frequency fluctuations. To achieve greater control over the frequency, a hierarchical control architecture for diesel generators is typically adopted in islanded microgrids, leveraging different time constants to cover both fast and slow dynamics [1], [2], [3].

Generally, hierarchical frequency control in microgrids involves primary and secondary controls [1]. The primary control is used to respond instantaneously to frequency

The associate editor coordinating the review of this manuscript and approving it for publication was Yifan Zhou.

variations, to resume operation based on reference values and enable active power sharing among generators. Among several control methods, droop control has been widely used as the primary control to regulate the frequency of multiple diesel generators in islanded microgrids [4], [5]. This control method stably shares the load between diesel generators by intentionally dropping the frequency reference in proportion to the increase in load. However, even if the frequency remains stable within a certain range, frequency deviation is inevitably induced as a result of the droop mechanism. To eliminate frequency deviation, an additional or ''secondary'' control method is required to restore the frequency to its nominal value [2].

For secondary control of the frequency, a centralized control structure, the microgrid central controller (MGCC), has been studied as a potential solution; this controller readjusts the load reference of diesel generators and restores the frequency to a nominal value [6], [7]. However, this structure requires additional equipment and may be exposed to a single point of failure risk, which can lead to system collapse [8], [9]. Even for more minor infractions, these issues can lead to degradation and/or failure of the system dynamics, which is not acceptable for systems where power quality is very important [10], [11]. Furthermore, cyber-layer attacks, such as denial of service (DoS), false data injection and replay attacks, can also cause physical-layer attacks, ultimately resulting in system collapse [12].

To overcome the issues associated with MGCCs, distributed and decentralized controls have been proposed. Distributed controls normally use consensus algorithms that communicate only with adjacent units to exchange signals [13], [14], [15]. With this approach, each unit communicates repeatedly with adjacent units until they converge. Therefore, this method can still be applied even if a communication failure occurs at some point. However, distributed control still requires complex analytical processes and remains vulnerable to severe communication failures, DoS, data dropout, time delays, false data injection, and measurement errors [15].

Although several methods have been proposed to address these problems [16], [17], [18], [19], [20], [21], [22], the attack models in each paper are assumed bounded, energy limited, or periodic signals. The [16] assumes that the time delay in the measurement device is bounded, meaning packets delayed beyond this limit are dropped. The maximum allowable delay in [16] is set to twice the sampling period, making the control unstable if delays exceed this threshold (∼few milliseconds) due to time source degradation attack, packet content manipulation attack, replay attack, and etc [23].

In [17], the DoS attack model is characterized by the lower and the upper bounds of sleep and active durations respectively while the DoS attack model in [18], [19], [20], and [21] are characterized by DoS frequency and duration. The [22] is also characterized by DoS duration with assumption that DoS attacks are energy-limited. Thus, if the DoS attack periods exceed the controller's affected period, the controller will be impacted by DoS attacks [21]. Historically, the primary obstacle to releasing the full potential of DoS attacks was the lack of resources available to attackers. However, with amplification-based DoS attacks in play, lack of resources can be overcome by using these types of attacks [24]. Consequently, the distributed control in [17], [18], [19], [20], [21], and [22], which assume bounded or energy-limited DoS attack models and validate performance under limited conditions, are vulnerable to modern intelligent DoS attackers.

As alternatives, decentralized integral control methods have been proposed for frequency regulation without the need for telecommunications [25], [26], [27]. Several decentralized control methods, such as pure integral control and linear quadratic regulator-based solutions [25], integral control with load change detection and a timing unit [26], and adaptive control with a power derivative term supplemented with droop control [27], have been proposed.

Although it is theoretically viable to apply such control methods to multiple generators, implementation is not practical for real power systems, due to unknown biased errors such as measurement and analog-to-digital (ADC) errors in the microcontroller. Even slight measurement errors can cause clock drift instability resulting in fighting among multiple generators [28], [29]. In other words, the generators swing back and forth until the reverse power relay of the unit, or the under-frequency relay actuates likely due to overgeneration. This phenomenon is discussed in detail in [30]. We further demonstrate why these decentralized methods cannot be implemented practically and show this phenomenon by controller hardware in the loop simulation (CHILS) in Section V.

To prevent clock drift between frequency controllers, [30] proposed a robust secondary frequency control (SFC) method. This method prevents clock drift even when there are unknown biased errors caused by the leaky integral controller. However, while this control successfully prevents clock drift, it results in a relatively large offset error in steady-state frequency, regardless of the occurrence of unknown biased errors [30]. Additionally, the offset error varies among operating points. Therefore, the large offset error induced by leaky integral control poses practical limitations in terms of restoring frequency in real power systems. In [31], a small-AC signal injection method has been proposed for grid-forming inverters, employing fourth order harmonic signals of the base frequency to address transient real power sharing mismatches caused by disturbances or noises in secondary PI control. However, intentionally generated fourth order harmonic signals may result in the malfunction of protective relays due to their operating principles [32].

This paper presents a novel decentralized SFC for multiple diesel generators, which restores frequency almost to the nominal value and achieves accurate power sharing between generators without clock drift. To eliminate frequency mismatch from primary control and prevent clock drift, a novel compensating method without any harmonic

signals is proposed for the conventional integration process applied during SFC. The main contributions of this article are listed as follows.

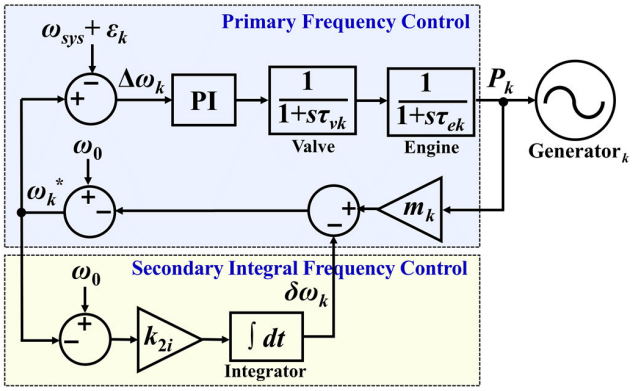

FIGURE 1. General schematic diagram of the primary and secondary frequency control loops for diesel generators.

1) The development of a novel frequency reference compensation method for decentralized SFC with only local measurement could properly handle the unknown measurement errors without clock drift while parallel operation of grid forming diesel generators.

2) To rigorously verify the system stability, this study employs small-signal stability analyses and the common quadratic Lyapunov method. These analyses are conducted with the formulation of switched state-space modeling of the proposed control, providing comprehensive insights into the stability characteristics of the proposed control system.

3) The heuristic optimization-based control parameter setting is adopted to achieve the optimal control parameters by minimizing the trace of the arbitrary positive definite matrix closely associated with system stability, thereby enhancing the overall control effectiveness.

The remainder of this paper is organized as follows. The analysis of the hierarchical control architecture is introduced in Section II. Section III describes the proposed secondary frequency controller. Section IV discusses the stability analyses in terms of switched state-space modeling with common quadratic Lyapunov function (CQLF) and the control parameter settings using particle swarm optimization which is heuristic optimization. Section V describes CHILS software simulation with Novacor which is a real-time digital simulator (RTDS), to verify the feasibility of the proposed method based on a real power system on Geocha Island in South Korea. Conclusions are presented in Section VI.

II. ANALYSIS OF THE HIERARCHICAL CONTROL ARCHITECTURE

Fig. 1 shows a general schematic diagram of the PFC in [33] and SFC loops in [26] for diesel generators when the measured system frequency, ω_{sys}, deviates from the nominal frequency ω_0. Note that the structure of the PFC and SFC are fully separated in the time response. The ω_{sys} corresponds to the rotational frequency of the rotor. ε_k is the inherent unknown biased error when ω_{sys} is measured at the kth generator. The ω_k^* is the frequency reference, and $\Delta\omega_k$ is the difference between the reference and measured frequencies, including the measurement errors of generator k. The m_k is the droop coefficient, P_k is the mechanical power, τ_{vk} and τ_{ek} are the valve actuator and engine time constant of the generator k, respectively.

A. OVERVIEW OF GOVERNOR CONTROL OF THE DIESEL GENERATOR

In case of a mismatch between the total mechanical power and load power, the frequency changes according to the swing equation, expressed as follows:

$$\Delta\omega_{sys} = \frac{1}{M_{eq}s + D}\left(\sum_{k=0}^{n}\Delta P_k - \Delta P_L\right), \tag{1}$$

where M_{eq} is the equivalent inertia constant, D is the load damping coefficient, ΔP_k is the mechanical power change of the kth generator, n is the number of generators, ΔP_L is the load change, 's' is the Laplace operator for frequency domain and $\Delta\omega_{sys}$ is the system frequency change [34].

When $\Delta\omega_{sys}$ changes, the input of each governor, $\Delta\omega_k$, changes in the opposite direction, as expressed by

$$\Delta\omega_k = \omega_k^* - (\omega_{sys} + \varepsilon_{\text{k}}). \tag{2}$$

The $\Delta\omega_k$ instantaneously changes the mechanical power of the generator output P_k by the proportional and integral (PI) control passing through the valve actuator and engine. The transfer function is expressed as

$$(\omega_k^* - \omega_{\text{sys}} - \varepsilon_k)(k_{1p} + \frac{k_{1i}}{s})(\frac{1}{1+s\tau_{vk}})(\frac{1}{1+s\tau_{ek}}) = P_k, \tag{3}$$

where k_{1p} and k_{1i} are the PI gains of the primary frequency control (PFC). This process balances the power in the steady state and allows for frequency regulation according to the frequency reference.

B. PRIMARY FREQUENCY CONTROL WITH MEASUREMENT ERROR

Active power sharing is necessary while ensuring power balance, such that the generators share loads proportional to their rated power. Primary frequency droop control can satisfy active power sharing by readjusting the frequency reference as follows:

$$\omega_k^* = \omega_0 - m_k P_k. \tag{4}$$

Therefore, PFC adjusts the ω_k^* in relation to P_k, and the governor regulates ω_{sys} according to ω_k^* via PI control. Thus, ω_k^* and ω_{sys} converge differently from the nominal frequency due to the droop mechanism in (4).

Primary droop control is fast and easy to implement; however, it has the major drawback of potential frequency deviation due to the droop mechanism. Thus, SFC is necessary to restore the frequency to its nominal value.

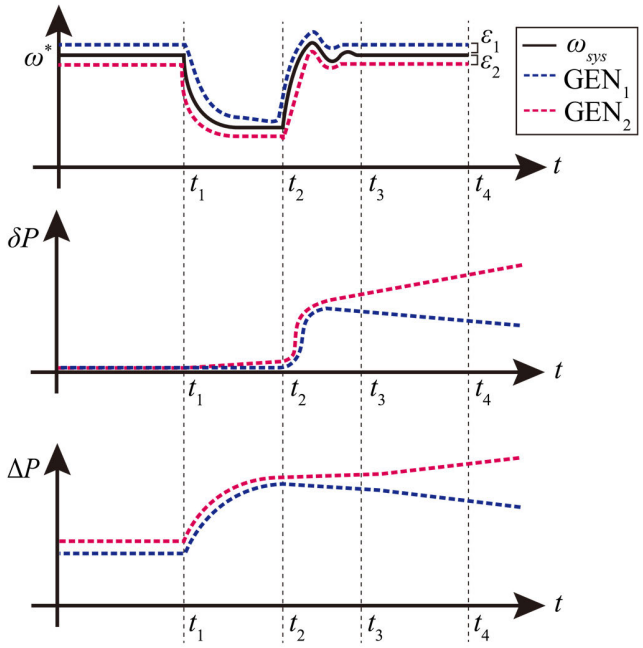

FIGURE 2. Waveforms of frequency reference ω_k^*, the term of SFC δP, and the active power ΔP of two generators during the frequency restoration process of SIFC with unknown measurement errors.

C. SECONDARY FREQUENCY CONTROL WITH ACCMULATED EERROR

SFC is necessary to eliminate the frequency deviation originating from the primary droop control. Implementing SFC transforms the frequency reference equation as follows:

$$\omega_k^* = \omega_0 - m_k P_k + \delta\omega_k, \tag{5}$$

where $\delta\omega_k$ is the frequency restoration term provided by the SFC. Various studies have proposed decentralized secondary integral frequency control (SIFC) to determine $\delta\omega_k$ and minimize the risk of telecommunication delays and cyber-physical attacks [25], [26], [27]. These studies adopted the integral control method to determine $\delta\omega_k$ for eliminating the frequency deviation, as follows:

$$\delta\omega_k(t) = k_{2i} \int_0^t (\omega_0 - \omega_k^*(\tau))\, \mathrm{d}\tau, \tag{6}$$

where k_{2i} is the integral gain of the SIFC.

Fig. 2 depicts the sketch waveforms of the ω^*, δP, and ΔP of generators 1 and 2 (GEN_1 and GEN_2) during the frequency restoration process considering unknown biased error (ω_1 and ω_2). Initially, ω_{sys} and ω^* are assumed to be equal to ω_0, and only the primary droop control is applied. Subsequently, the step load increases at $t = t_1$, and ω_{sys} is decreased according to (1). SFC is applied at $t = t_2$ to observe the clock drift phenomenon of the active power of the two generators. From $t = t_2$, ω_{sys} and ω^* recover up to ω_0, whereas the δP and ΔP of GEN_1 and GEN_2 increase or decrease in opposite directions. Fig. 3 shows the trends of the operating points with respect to the P-ωcurve to effectively demonstrate the changes after SIFC is applied to the two generators. To evaluate the clock drift phenomenon after applying SFC, P_1 and P_2 are assumed to be equal, and only PFC with the ω_{pri} which is the converged frequency reference only after the PFC and measurement noises (ε_1 and ε_2) are considered.

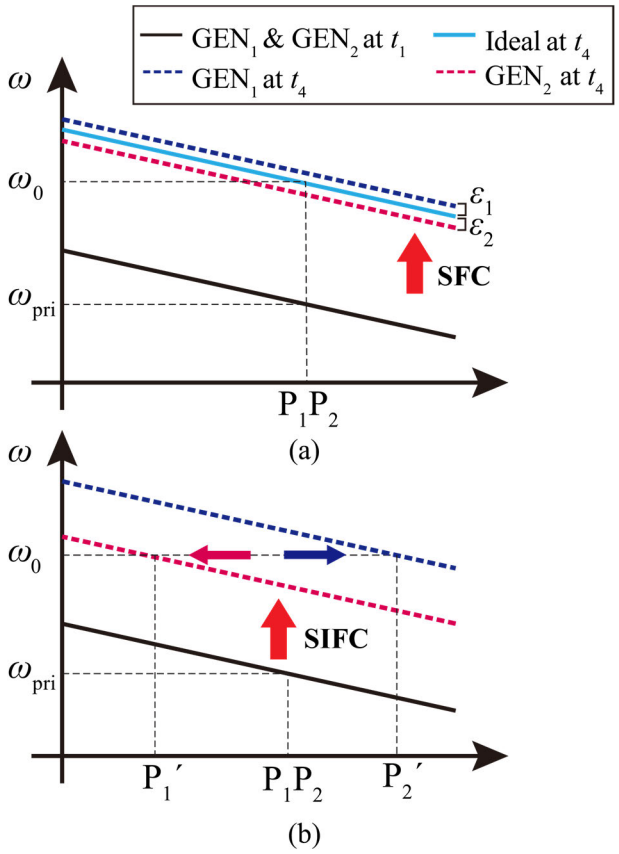

FIGURE 3. *P-ω* curve operating points of two generators during SFC with (a) the expected ideal case and (b) the SIFC method.

Fig. 3(a) shows the expected results when the SFC operates as intended. The figure shows that ω_1^* and ω_2^* converge near ω_0 with minimal difference proportional to noises, and P_1 and P_2 converge to similar operating point. However, with the SIFC method shown in Fig. 3(b), although ω_1^* and ω_2^* converge near ω_0, perfect convergence to ω_0 is difficult to achieve due to unknown biased errors. Thus, $\delta\omega_1$ increases cumulatively owing to the mismatch between ω_1^* and ω_0. Conversely, the governor of generator 1 reduces P_1 owing to the negative value of $\Delta\omega_1$ derived from (2), and δP_1 decreases as well. ω_1^* can converge to a specific point near ω_0 owing to the zero-sum between the increasing term from the product of m_1 and P_1 and the decreasing term from (6), whose δP and ΔP are shown in Fig. 2. The same process applies to GEN_2 but in the opposite direction. Thus, although ω_1^*, ω_2^*, and ω_{sys} appear to converge without problems, P_1 decreases

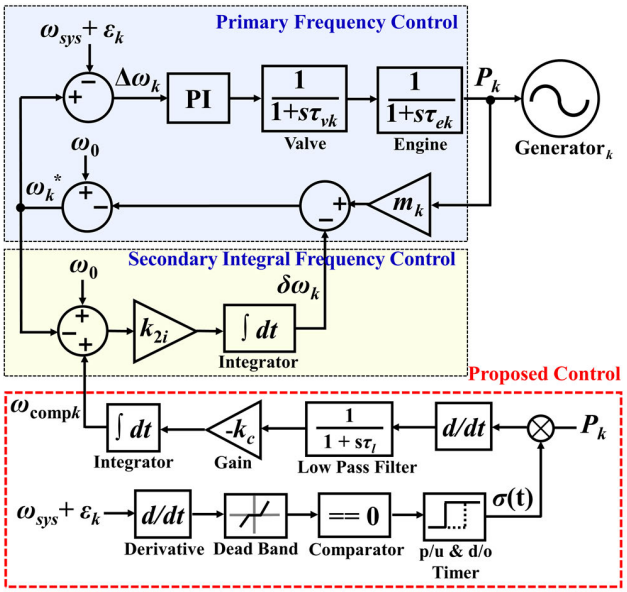

FIGURE 4. Schematic diagram of the proposed frequency reference compensation control.

until the reverse power relay is tripped, while P_2 increases until the overcurrent relay is tripped. Hence, unknown biased errors cause instability in the system due to clock drift, i.e., generator fighting occurs [30], [31].

To prevent such issues, generators must have the same settings to eliminate biased errors [34]. However, in an actual power system, regardless of how many attempts are made to set the control parameters to be identical, achieving perfectly identical frequency settings is virtually impossible. Measurement errors are inevitable in any frequency measurement method [35]. Moreover, devices of the same model and measuring points may still yield different values. Furthermore, errors can occur in the ADC converters of microcontrollers, such as gain and offset errors. Therefore, frequency errors between the reference and measurement in two or more governors cannot be perfectly controlled without eliminating measurement or microcontroller errors.

III. FREQUENCY REFERENCE COMPENSATION CONTROL

This section presents the proposed novel SFC method for preventing clock drift. First, the conditions that lead to clock drift were identified. Clock drift occurs when the frequency derivative $d\omega_{sys}/dt$ is approximately zero, resulting in an increase or decrease in the mechanical power derivative dP_k/dt. A constant frequency implies that power balance is achieved based on the time-domain form of (1), expressed as

$$\frac{d\Delta\omega_{sys}}{dt} = \frac{1}{M_{eq}}\left(\sum_{k=0}^{n}\Delta P_k - \Delta P_L - \mathrm{D}\Delta\omega_{sys}\right). \quad (7)$$

Although power balance is achieved, some generators tend to exhibit an increasing change in power (due to larger $\Delta\omega_k$); conversely, other generators exhibit a decreasing change in power with an opposite trend owing to the inherent biased errors ε_k among generators with different values, as shown in Fig. 3. The equation is transformed by substituting (2) into (3) and converting the equation into the s' domain.

$$(\Delta\omega_k)(sk_{1p} + k_{1i})\left(\frac{1}{1+s\tau_{vk}}\right)\left(\frac{1}{1+s\tau_{ek}}\right) = sP_k. \quad (8)$$

Because clock drift occurs when $d\omega_{sys}/dt$ is zero, the sk_{1p} term can be ignored, and $\Delta\omega_k$ becomes proportional to sP_k, i.e, dP_k/dt in time domain, derived from (8). Therefore, $\Delta\omega_k$ should converge to zero to regulate frequency without clock drift.

To achieve this, this study proposes a frequency reference compensation control (FRCC) method for the SFC, as shown in Fig. 4, which can be expressed as

$$\delta\omega_k(t) = k_{2i}\int_0^t \left(\omega_0 - \omega_k^*(\tau) + \omega_{compk}(\tau)\right)d\tau. \quad (9)$$

In the conventional SFC term of (6), the proposed compensation term, $\omega_{\mathrm{comp}k}$, is added and restores ω_k^* in (5). Considering that $\Delta\omega_k$ is proportional to dP_k/dt, $\omega_{\mathrm{comp}k}$ should have the opposite sign of dP_k/dt and is integrated from (9) to make $\Delta\omega_k$ in (8) zero. Thus, the proposed compensation term $\omega_{\mathrm{comp}k}$ is derived as follows:

$$\omega_{compk} = -\frac{k_c}{s}\frac{1}{1+s\tau_l}\frac{dP_k}{dt}, \quad (10)$$

dP_k/dt passes through a low-pass filter, which smooths out rapid and frequent changes in the time constant τ_l. ω_k^* is adjusted through compensation and integration, such that $\Delta\omega_k$ approaches zero. The value of $\omega_{\mathrm{comp}k}$ is derived as the negative integral of the low-pass filter output multiplied by the constant k_c. Note that this parameter should be sufficiently small to prevent the frequency reference from deviating too far from the nominal value, which could negatively affect control stability.

To prevent the controller from undergoing frequent changes, ω_{compk} readjusts the frequency reference ω_k^* under the following conditions:

$$\sigma(t) = \begin{cases} 1, & \frac{d\omega_m}{dt} < DB_{th} \\ 0, & \frac{d\omega_m}{dt} > DB_{th} \end{cases} \quad (11)$$

where DB_{th} is the threshold of the deadband, and σ(t) is the control signal that determines whether the FRCC should be activated. When the signal σ(t) is equal to 1 at the kth generator, the values of $\omega_{\mathrm{comp}k}$ are adjusted according to (10). $\omega_{\mathrm{comp}k}$ decreases when the mechanical power increases at the kth generator. Conversely, $\omega_{\mathrm{comp}k}$ increases when the mechanical power decreases.

Through the condition in (11), the deadband allows the controller to operate only when the frequency derivative is sufficiently small to determine whether power balance is achieved. However, the FRCC can be activated even when $d\omega_{sys}/dt$ is momentarily zero during the transient response of governor control. This can result in a relatively large $\omega_{\mathrm{comp}k}$

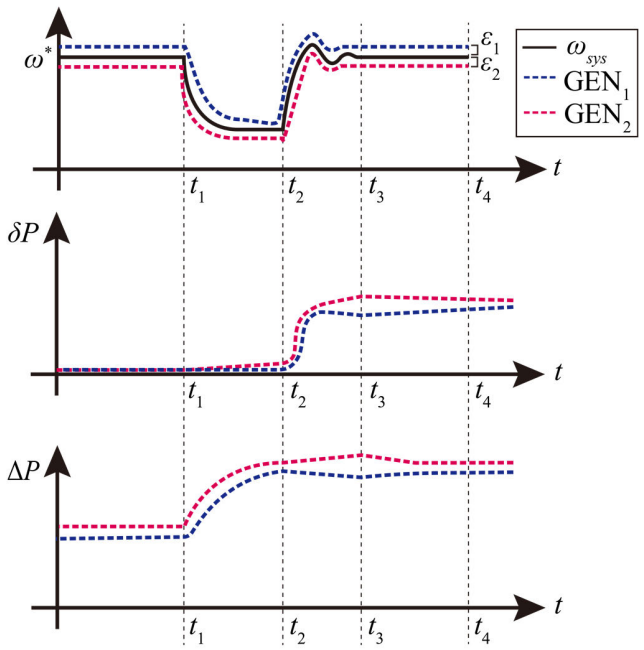

FIGURE 5. Sketch waveforms of frequency reference ω_k^*, the term of SIFC δP and the active power ΔP of two generators during frequency restoration process of proposed frequency reference compensation methods with unknown measurement errors.

due to the large dP_m/dt, causing ω_k^* to deviate from the nominal value. To prevent this, a pick-up and drop-out (p/u & d/o) timer is implemented in Stage (11). This renders σ(t) equal to 1 only when the condition in (11) is satisfied for longer than a preset time interval.

Via the proposed SFC, $\omega_{\text{comp}k}$ compensates for ε_k such that the accumulated error is eliminated. Accordingly, ω_k^* converges to $\omega_{sys} + \varepsilon_k$, and $\omega_0 + \omega_{\text{comp}k}$. In other words, the sum of the input variables of the governor $(\omega_k^* - \omega_{sys} - \varepsilon_k)$ in (2) and inner part of the SFC $(\omega_0 - \omega_k^* + \omega_{\text{comp}k})$ in (9) is equal to zero. Therefore, clock drift is prevented in the governors of the generators, and the frequency is controlled close to a nominal value.

As shown in Fig. 5, the SIFC reduces δP_1 and ΔP_1 between t_2 and t_3. The proposed FRCC is activated when the condition in (11) is satisfied ($t = t_3$), causing the δP_1 and ΔP_1 to increase and finally converge. Therefore, as shown in Fig. 6, the operating points of the two generators at $t = t_4$ converge with minimal mismatch proportional to ε_1 and ε_2, and ω_1^* and ω_2^* approach ω_0. This mismatch is negligible because the unknown biased error is bounded and sufficiently small to minimize the mismatch in an actual setting [36], [37]. Notably, even the expected ideal case has a mismatch between P_1 and P_2, as shown in Fig. 3(a).

IV. FREQUENCY REFERENCE COMPENSATION CONTROL

This section compares the stability of the SIFC in [25], [26], and [27] with that of the proposed FRCC via switched state-space modeling. The generator parameters were selected

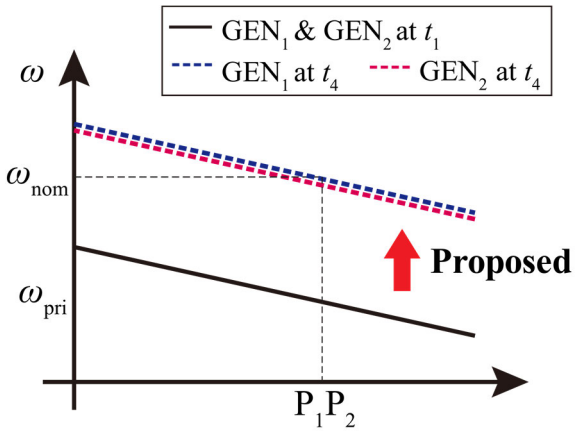

FIGURE 6. *P-ω* curve operating points of two generators during proposed FRCC method.

TABLE 1. Control and model parameters of two diesel generators.

Type	Parameter	Symbol	Value	Units
Diesel generator	Inertia coefficient	M_1, M_2	3.174, 5	s
	Load-damping coefficient	D	0.01	-
	LPF cutoff frequency	τ_{v1}, τ_{e1}, τ_{v2}, τ_{e2}	0.05, 0.5, 0.1, 1.0	s
	Droop coefficients	m_1,m_2	0.02, 0.015	Hz/kW
	Primary PI gains	k_{1p}, k_{1i},	6.7, 3.2	- , 1/s
	Secondary integrator gain	k_{2i}	1.0	1/s
Proposed control	Deadband threshold	DB_{th}	±0.0025	-
	LPF cutoff frequency	τ_l	1.76	s
	Integral gain	k_c	0.5	1/s

from Table 1 to verify the stability of the generators. The design of the proposed control parameters is discussed to ensure the accuracy of the proposed model.

A. STATE-SPACE MODELING OF FREQUENCY CONTROL OF GENERATORS

The transfer function of the general frequency control structure in generator k can be expressed as (3). To simplify the calculation, the denominators are removed and expressed as small-signal terms.

$$\begin{aligned}&(\Delta\omega_k^* - \Delta\omega_{\text{sys}} - \Delta\varepsilon_k)(sk_{1p} + k_{1i})\\ &= s\{(\tau_{vk}\tau_{ek})s^2\\ &\quad + (\tau_{vk} + \tau_{ek})s + 1\}\Delta P_k,\end{aligned} \tag{12}$$

where $\Delta\omega_k^*$ is defined in (5) and (6). Note that $\Delta\omega_{\text{comp}k}$ is considered only in the proposed method. To analyze the dynamics of the state variables, including ω_{sys} and P_m, the Laplace equation given in (12) is transformed into the time

domain, yielding

$$\Delta\dddot{P}_k = \frac{1}{\tau_{vk}\tau_{ek}}\{-(\tau_{vk}+\tau_{ek})\Delta\ddot{P}_k - \Delta\dot{P}_k + k_{pk}(\Delta\dot{\omega}_k^* - \Delta\dot{\omega}_{sys} - \dot{\varepsilon}_k) + k_i(\Delta\omega_k^* - \Delta\omega_{sys} - \varepsilon_k)\}. \quad (13)$$

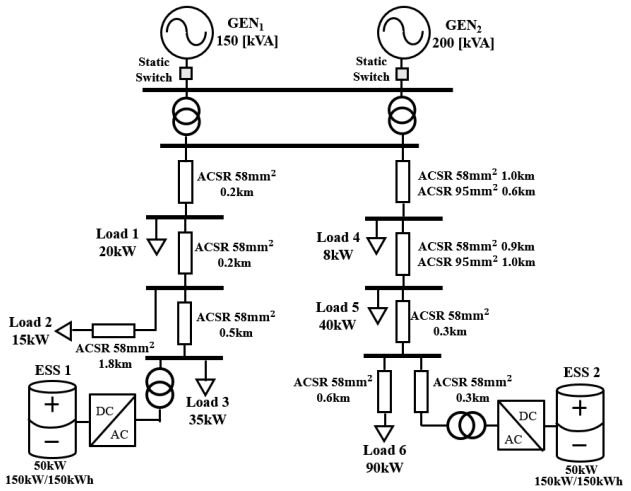

FIGURE 7. Overall schematic diagram of a real power system in Geocha Island, South Korea.

The differential equation in (13) is derived individually for each generator; these equations, including (7), can be expressed as a state-space equation.

$$\Delta\dot{\mathbf{x}} = \mathbf{A}_{gen}\Delta\mathbf{x} + \mathbf{B}_{gen}\Delta\mathbf{u}, \quad (14)$$

where $\mathbf{A}_{gen}$ is the system matrix, $\mathbf{B}_{gen}$ is the input matrix, $\Delta\mathbf{x}$ is the state vector, $\Delta\dot{\mathbf{x}}$ is the derivative of $\Delta\mathbf{x}$, and $\Delta\mathbf{u}$ denotes uncontrollable input vectors, such as loads and errors. The system is stable if and only if all real parts of the eigenvalues of $\mathbf{A}_{gen}$ are less than zero. In this study, the state-space equations of the two generators in Fig. 7 with the parameters in Table 1 were applied, where $\Delta\mathbf{x} = [\Delta\omega_{sys}, \Delta\omega_{ref1}, \Delta P_1, \Delta\dot{P}_1, \Delta\ddot{P}_1, \Delta_{ref2}\ \Delta P_2, \Delta\dot{P}_2, \Delta\ddot{P}_2]^T$, and $\Delta\mathbf{u} = [\Delta P_L, \Delta\varepsilon, \Delta\dot{\varepsilon}]^T$.

Here, state variables $\Delta\dot{P}_1$ and $\Delta\ddot{P}_1$ and $\Delta\dot{P}_2$ and $\Delta\ddot{P}_2$ are the first and second derivatives of the mechanical power of generators 1 and 2, respectively. A comprehensive explanation of these matrices is provided in the Appendix.

The eigenvalues of the system matrix are represented as a root-locus plot in Fig. 8, representing the eigenvalues of the SIFC system without the proposed compensation. The figure shows that the real parts of the eigenvalues are on the negative side and zero. Even if the real parts of all eigenvalues of the system are less than or equal to zero, one eigenvalue at the critical point cannot ensure system stability. Participation factors (p_{ij}) can be introduced, as in [38], to analyze the state variables correlating with the eigenvalue at the critical point

$$p_{ij} = \frac{|w_{ij}|\,|v_{ji}|}{\sum_{k=1}^{N}(|w_{ik}\|v_{ki}|)}, \quad (15)$$

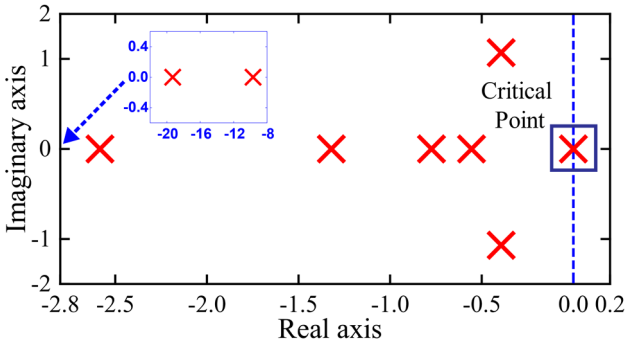

FIGURE 8. Root-locus plot of the eigenvalues of the conventional system matrix.

TABLE 2. Grid model parameters.

Type	Parameter	Symbol	Value	Units
Generators	Diesel generator Capacity	S_{rate1}, S_{rate2}	150, 200	kVA
	ESS Capacity	P_{ess_rate1}, P_{ess_rate2}	100, 100	kW
	Active power of ESS	P_{ess1}, P_{ess2}	34, 34	kW
	ESS inner current loop of PI gains	i_{kp}, i_{ki}	0.2, 0.30675	
Line Impedance	ACSR 58 mm²		0.497+j0.438	Ω/km
	ACSR 95 mm²		0.304+j0.420	Ω/km

where the ith state and jth eigenvalue are associated with the left (w_{ij}) and right eigenvectors (v_{ij}), respectively [38]. A higher participation factor implies a stronger correlation between the corresponding eigenvalue and state [39]. The participation factors corresponding to the eigenvalues at the critical point are as follows:

$$p_{ij(\lambda_j=0)} = [\,\mathbf{O}_{1\times2}\ 0.5\ \mathbf{O}_{1\times3}\ 0.5\ \mathbf{O}_{1\times2}\,^T], \quad (16)$$

where $\mathbf{O}_{1\times2}$ is the zero matrix comprising one row and two columns. These participation factor values indicate that only state variables ΔP_1 and ΔP_2 are correlated with the eigenvalue at the critical point. Thus, excluding ΔP_1 and ΔP_2, the state variables in $\Delta\mathbf{x}$ were asymptotically stable.

B. STABILITY ANALYSIS OF THE PROPOSED CONTROLLER WITH EIGENVALUES

The pole at zero in the SIFC should be shifted to the negative side to ensure system stability. The pole at zero was relocated to the negative side by applying the frequency reference compensation through the proposed control, as shown in Fig. 9. The proposed control equation given in (10) can be transformed into the following differential equation:

$$\dot{\omega}_{compk} = -\frac{k_c}{\tau_l}\Delta P_k - \frac{1}{\tau_l}\Delta\omega_{compk}. \quad (17)$$

The state-space model of the proposed controller must be modeled as a switched linear system because it has two states (active/inactive). It operates only under specific conditions

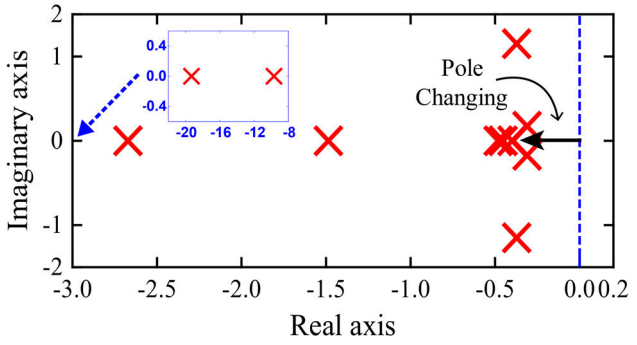

FIGURE 9. Root-locus plot of the eigenvalues of the conventional system matrix.

given by (11). The state-space equation of the proposed controller is as follows:

$$\dot{\mathbf{X}} = \mathbf{A}_{\sigma(t)} \cdot \mathbf{X} + \mathbf{B}_{\sigma(t)} \cdot \mathbf{U} \tag{18}$$

where $\mathbf{X}$ is the state vector, the same as $\Delta\mathbf{x}$, including $[\Delta\omega_{\text{comp1}}, \Delta\omega_{\text{comp2}}]^T$, $\mathbf{U}$ is the uncontrollable input matrix, the same as $\Delta\mathbf{u}$, $\mathbf{A}_{\sigma(t)}$ is the switched system matrix, and $\mathbf{B}_{\sigma(t)}$ is the switched input matrix that depends on the parameters of $\sigma(t)$. When $\sigma(t)$ is equal to 0, it corresponds to the system shown in (14), denoted as $\mathbf{A}_{\sigma(t)=0}$, the same as $\mathbf{A}_{gen}$. Conversely, when $\sigma(t)$ is equal to 1, it corresponds to the proposed control system shown in Fig. 4; therefore, the system matrix is transformed from $\mathbf{A}_{\sigma(t)=0}$ to $\mathbf{A}_{\sigma(t)=1}$, the same as $\mathbf{A}_{\sigma(t)=0}$, but includes the terms in (17); i.e., $\mathbf{A}_{\sigma(t)=1}$ has additional eigenvalues. Due to the proposed compensation, as shown in Fig. 9, which is the root locus of the proposed controller, the eigenvalues at zero shift to the left side of the real axis. Thus, the matrix of the proposed frequency controller is asymptotically stable.

In summary, the proposed control system is a switched linear system with two system matrices, denoted as $\mathbf{A}_{\sigma(t)=0}$ and $\mathbf{A}_{\sigma(t)=1}$. These matrices are complementary and are activated or inactivated by the switching signal $\sigma(t)$. Based on Fig. 8, $\mathbf{A}_{\sigma(t)=0}$ has an eigenvalue at a critical point, which may cause system instability. However, based on the computed participation factors, the state variable $\Delta\omega_{sys}$ is verified to be asymptotically stable; i.e., $d\omega_{sys}/dt$ converges to zero. Thus, the signal $\sigma(t)$ should approach 1 asymptotically. This indicates that the multiple diesel generators converge to the $\mathbf{A}_{\sigma(t)=1}$ system matrix when using the proposed controller. Therefore, the proposed compensator stabilizes an unstable system. Section IV-C describes the CQLF to further prove the stability of the switched system.

C. COMMON QUADRATIC LYAPUNOV METHOD AND SETTING AND CONTROL PARAMETERS

The existence of a CQLF in a switched system is a necessary and sufficient condition to ensure the asymptotic stability of the system for any switching signal [40]. For system (18), let

Algorithm 1 PSO Algorithm for k_c and τ_l

```
Initialize PSO parameters: N_particle, v_0, γ, l_max
Initialize system parameters in Table 1.
Generate particles and velocity: p = (k_c0, τ_l0) and v
For l < l_max do
    | Update the v and position of p with γ
    | Evaluate particles with fitness function (21)
    | update p_best', g_best within particles
    # Run SDP Program
    | Update A_σ(t)=1 with p_best'
      | Solve SDP optimization
        | objective : min(tr(P))
        | subject to:
          | P > 0, Q > 0
          | A^T_σ(t)=0 P + P A_σ(t)=0 < -Q
          | A^T_σ(t)=1 P + P A_σ(t)=1 < -Q
      | If P exists :
        | update p_best = p_best'
        |l = l + 1
      | If p_best changes:
        |l = 0
    End For
    k_c, τ_l = p_best
    Output: k_c, τ_l
```

the scalar function CQLF be

$$V(\Delta\mathbf{x}) = (\Delta\mathbf{x})^T \mathbf{P}(\Delta\mathbf{x}), \tag{19}$$

where $\mathbf{P}$ is a positive-definite matrix. To ensure the system stability, the $\dot{V}$, the derivative of V, should be negative definite matrix, i.e., the sufficient condition is denoted as

$$\sum_{\sigma} (\mathbf{A}_{\sigma}^T \mathbf{P} + \mathbf{P}\mathbf{A}_{\sigma} + \mathbf{Q} < 0), \tag{20}$$

where $\mathbf{Q}$ is a positive-definite matrix. It satisfies $\lim_{x\to\infty} \mathrm{V(x)} <= \rho$, where ρ is arbitrary positive constant; i.e., the system is asymptotically stable. The condition expressed in (20) for a CQLF is formulated as a linear matrix inequality (LMI), and its existence is verified using semidefinite programming (SDP). This study employed the MOSEK solver in conjunction with the CVXPY modeling language implemented in Python for SDP.

The design of the control parameters outlined in (17) significantly affected the performance of the proposed FRCC. Therefore, a heuristic optimization method called particle swarm optimization (PSO) was employed to find the optimal control parameters k_c and τ_l due to its advantage of having few setting parameters and fast convergence [16]. First, the PSO parameters are initialized, where N_{particle} is the number of particles, v_0 is initial velocity, γ is the weighting coefficients for each particle p, and $l_{\max}$ is the maximum number of iterations. At the end of the condition of the PSO algorithm, the global best position of the particle, g_{best}, does not change for more than iteration $l_{\max}$. Subsequently, the system parameters in Table 1 are initialized, except the target variables of the algorithm k_c and τ_l. The iterations of the PSO algorithm commence after generating the initial particle and velocity. The fitness function for evaluating each iteration is

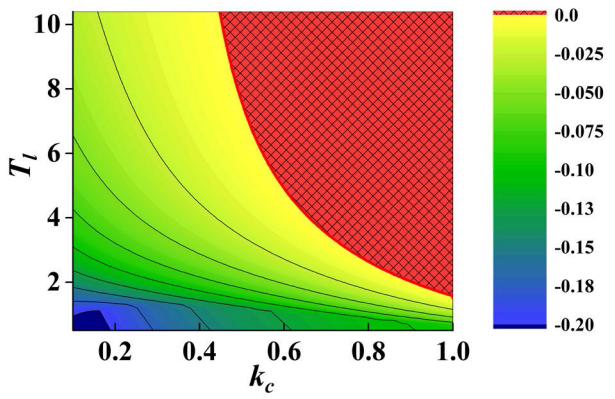

FIGURE 10. λ_{max} distribution of the system matrix with respect to parameters k_c and τ_l.

defined as follows:

$$J = \mu_1 J_1 + \mu_2 J_2, \tag{21a}$$

$$J_1 = \sum_{t=t_0}^{t_{end}} |\Delta\omega_{sys}(t)|, \tag{21b}$$

$$J_2 = \sum_{k}^{N_{gen}} \sum_{t=t_0}^{t_{end}} |\Delta P_k(t) - \Delta P_{av}|, \tag{21c}$$

$$\Delta P_{av} = \sum_{k}^{N_{gen}} |\Delta P_k(t)|/N_{gen}, \tag{21d}$$

where μ_1 and μ_2 are the weight coefficients of the objective functions J_1 and J_2, respectively. When the step load changes from t_0 to t_{end}, J_1 is calculated as the total sum of the changes in frequency, and J_2 is calculated as the difference between the total sum of the active power changes of the generators and their average. Thus, considering the importance of frequency control compared with that of active power sharing in secondary control, μ_1 and μ_2 are set to 10.0 and 1.0, respectively. The global best position before checking the stability via SDP and each best position of the particles, denoted as $g_{\text{best}}{}'$ and p_{best}, respectively, are updated after evaluating the fitness function. While updating the global best position of the particles, the existence of the CQLF in the switched system is verified through SDP for system stability, where tr($\mathbf{X}$) denotes the trace of $\mathbf{X}$ for an arbitrary matrix $\mathbf{X}$. $\mathbf{X}>0$ indicates that $\mathbf{X}$ is a positive-definite matrix, and $\mathbf{X}<0$ implies that $\mathbf{X}$ is a negative definite matrix. If P exists, g_{best} is updated to $g_{\text{best}}{}'$, otherwise, it remains unchanged. The final g_{best}, considered as optimal k_c and τ_l, are computed as [0.05, 1.76] using the PSO in Algorithm 1.

In Fig. 4, the thresholds of the deadband and timer settings are crucial to the proposed control approach and are directly related to control performance. The deadband ensures that the proposed control operates only under steady-state conditions. Based on [41], a reasonable definition of the steady state corresponds to the state in which the response value reaches and stays within 2% of the final value. Therefore, if the value within the parentheses in (7) is less than 0.02, the power mismatch between the mechanical power and load power is less than 2%. Thus, based on the equivalent inertia constant M_{eq}, equivalent to the sum of the inertia constants of the generators in Table 1, DB_{th} is set to $\pm$ 0.0025 p.u., such that the frequency reference compensation controller operates only when the mismatch between the mechanical power and load power is less than 2%.

The p/u and d/o timer must be set to prevent the proposed controller from activating during a transient response. To set the timer, the system time constant should be designed to activate the proposed controller only when the frequency response is in a steady state and is calculated to be 0.091 based on [40]. If the settling time (time to reach a steady state) is defined as the time required for the response to reach 2% of the final value, then the settling time is four times the value of the system time constant. Furthermore, the frequency derivative, $d\omega_{sys}/dt$, is measured as the average value over each 0.1 s interval, considering the standards in [42]. Thus, the time is set to 0.4 s to determine when the controller activates/deactivates when the four samples are within the deadband threshold.

D. FURTHER CONSIDERATIONS ON SETTING THE INITIAL POINTS IN THE PSO ALGORITHM

The convergence of the optimal solution of the PSO algorithm depends on the initial point [43]. To address this problem, the search space of the parameters was limited based on theoretical principles. The eigenvalue stability of the system was leveraged to determine the range of the designed parameters, as shown in Fig. 9. This is imperative because the derived parameters must satisfy the stability criteria of the system. When the parameters k_c and τ_l change, the vulnerable eigenvalue, $\lambda_{\max}$, also changes.

Fig. 10 shows the $\lambda_{\max}$ distribution of the system matrix with respect to parameters k_c and τ_l. When the $\lambda_{\max}$ for a specific k_c and τ_l is less than zero, the system is considered asymptotically stable. Fig. 9 indicates that the lower the parameters, the more stable the system. However, selecting these parameters presents a trade-off between stability and performance. Larger k_c and smaller τ_l values result in the rapid response of the proposed FRCC but increases instability. Conversely, smaller k_c and larger τ_l values result in a slow response but better stability. Therefore, the search space range of the PSO parameters were confined within a stable region, where k_c ranges from 0.001 to 0.6, and τ_l ranges from 0.1 to 5.0.

Subsequently, the initial particles were distributed either completely randomly or at regular intervals, where $N_{\text{particles}}$(number of particles for the PSO algorithms) was equal to 50. Consequently, the outcomes of the k_c and τ_l derived using the PSO algorithm in both cases were determined to be 0.5 and 1.76, respectively. These results are consistent with those of the grid search approach (GSA),

a robust and widely used method for ensuring a global solution but requires high computational time [44].

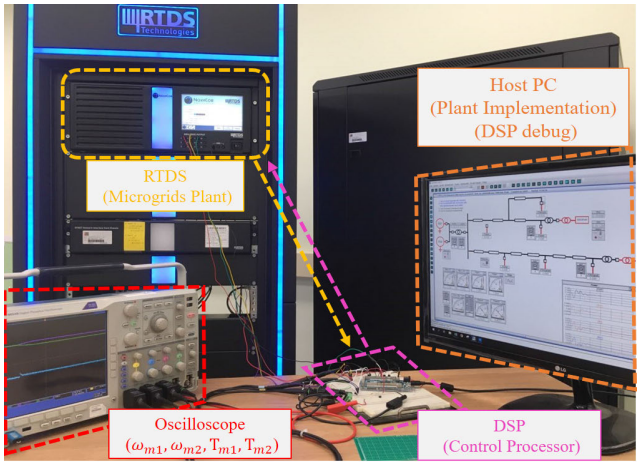

FIGURE 11. Simulation and controller hardware-in-the-loop simulation (CHILS). environment.

V. CHILS VERIFICATION

CHILS, a widely used method for practical verification of control methods, was used to verify the practical feasibility of the proposed control method. Fig. 11 shows the overall structure of the CHILS environment. Three secondary frequency control methods (SIFC, leaky integral control, and the proposed FRCC) were implemented using Atmel ARM Cortex-M3 core-based digital signal processor (DSP) boards and verified through microgrid simulations. The test microgrid plant shown in Fig. 7 was modeled in an RTDS to demonstrate the controllers in real time for more effective verification. Moreover, the host personal computer compiled and debugged the code for the SFC, which was programmed and implemented on DSP boards, and monitored the microgrid modeled in the RTDS. When the simulation test began, the RTDS sent the frequency signals of the two generators to the DSP boards and received the torque value signals from the boards through an I/O interface. An oscilloscope (DPO 4054B) was used to capture the measured frequency and mechanical torque signals (ω_{m1}, ω_{m2}, T_{m1}, T_{m2}) between the RTDS and MCU boards, where ω_{mk} and T_{mk} are expressed as

$$\omega_{mk} = \omega_{sys} + \varepsilon_k, \tag{22a}$$

$$T_{mk} = \frac{1}{\omega_{mk}} \frac{P_k}{P_{k,rated}}. \tag{22b}$$

To reduce the noise of the I/O signals in the DSP boards, a digital second-order Chebyshev filter was implemented during the subsequent stage; that is, the input signals were transferred from the ADC to the DSP boards. Table 1 lists the parameters for the two generators and controllers. The following scenarios were used for the CHIL tests: Only primary droop control was operated online for up to 10 s. At 10 s, secondary control methods were activated. At 50 s, a 20 kW load was applied to verify control in the transient state.

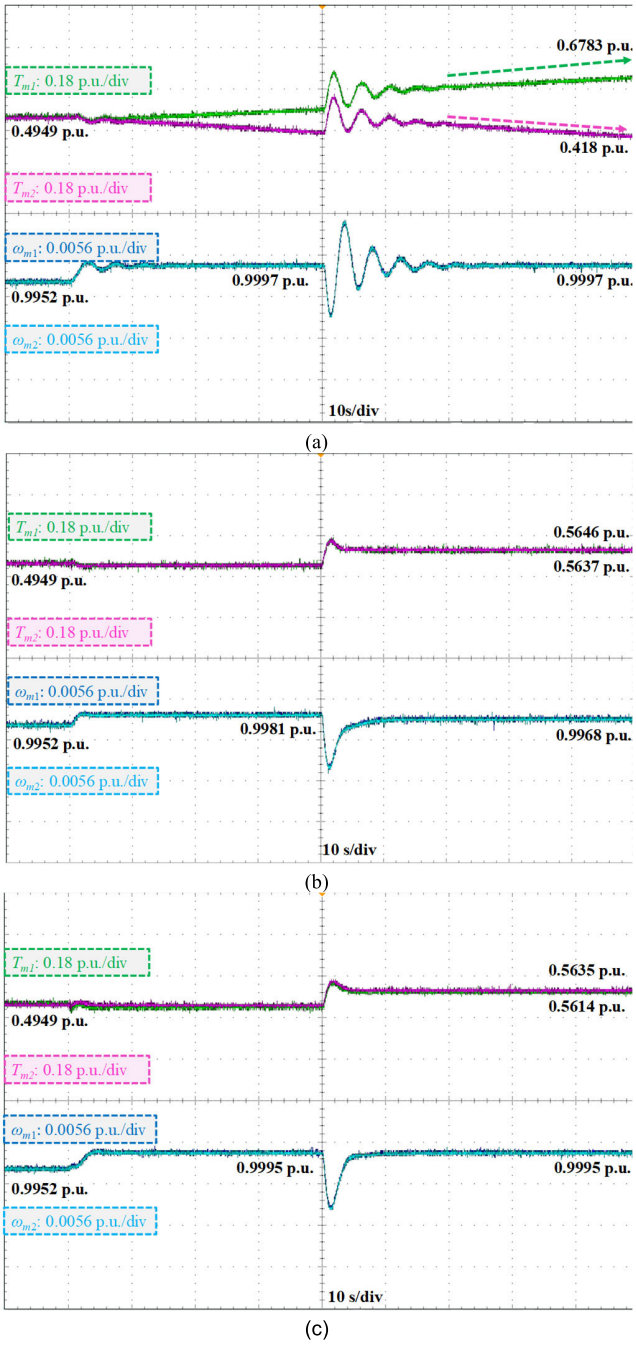

FIGURE 12. Secondary frequency control results of CHILS, in which the load increased by 20 kW at 50 s: (a) integral control, (b) leaky integral control, and (c) proposed frequency compensation control.

Fig. 12(a) shows the active power outputs of the diesel generators and the frequency of the system when the conventional integral control [23], [24], [25] was implemented. As shown in Fig. 12, the frequency was 0.9952 p.u. when the CHILS started and changed to 0.9997 p.u. after the integral controller was activated. The integral controller had to set the frequency to a nominal value in the absence of biased errors. Thus,

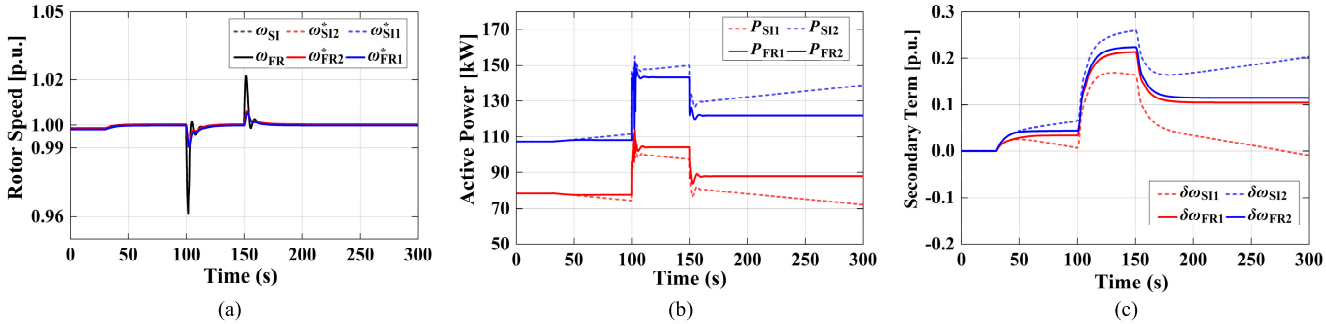

FIGURE 13. Comparison between the conventional SIFC and proposed FRCC with respect to sudden load disturbances: (a) system frequency and frequency reference, (b) active power, (c) frequency restoration term ($\delta\omega_k$).

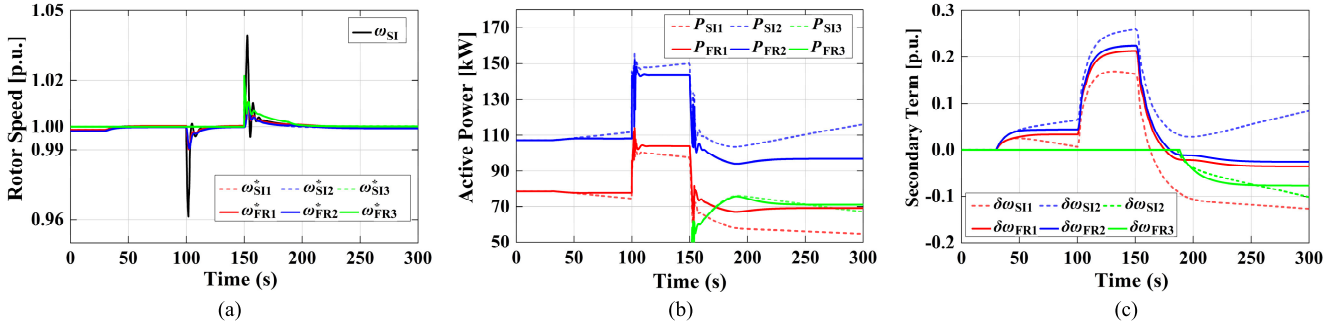

FIGURE 14. Comparison between the conventional SIFC and proposed FRCC with respect to plug and play: (a) system frequency and frequency reference, (b) active power, (c) frequency restoration term ($\delta\omega_k$).

the results demonstrated that average unknown biased errors of approximately 0.0003 p.u. are inherent to the microcontrollers and I/O devices, even those that were not intentionally applied to the test system. Consequently, the mechanical torque of diesel generator 1 increased continuously, whereas that of diesel generator 2 decreased continuously in the steady state until the relays tripped.

Fig. 12(b) shows the active power outputs of the diesel generators and the frequency of the system when the leaky integral control in [30] was implemented. The results also indicated that unknown errors occurred with slight changes in the frequency and torque at approximately 10 s. The frequency reached a steady state at 0.9981 p.u., and the generator torques converged. After a load disturbance at 50 s, the torques of the generators approached 0.5646 and 0.5637 p.u., and the frequency converged to 0.9968 p.u. These results revealed the systemic limitations of leaky integral control and the relatively large frequency deviation in the steady state and different converging frequencies among operating points.

Finally, Fig. 12(c) shows the active power outputs of the diesel generators and the frequency of the system when the leaky integral control was implemented. As shown in Fig. 11, the frequency and torque of the generators did not change in steady state. When the load was increased at 50 s, the controller increased the torque to regulate the frequency according to the nominal value. Furthermore, unlike in Fig. 12(a), clock drift between multiple frequency controllers did not occur; thus, the torques of the two generators did not change in opposite directions in the steady state. Nevertheless, a small torque mismatch between generators 1 and 2 was observed, similar to the results shown in Fig. 12(b). This mismatch was attributed to the variations among measurement devices, differences in the response delay, or different ADC gains and offset errors in the MCU boards. However, the proposed controller maintained the frequency close to the nominal value by compensating for unknown errors in the frequency reference. A compensation value of 0.0002 p.u., is negligible [34], [35]. Thus, even if the two generators have different rated powers and time constants, the frequency and torque converged successfully without clock drift with the proposed method, unlike with the conventional integral and leaky integral control approaches.

VI. SIMULATION RESULTS

Simulations involving various scenarios, such as sudden load changes, plug-and-play, and adopting FRCC to ESSs, were performed to verify the proposed FRCC in an islanded microgrid. The real power system described in Fig. 7 was modelled in the RTDS for software simulation with some modifications, including two generators and two ESSs. In this schematic, the diesel generators, whose parameters are listed in Table 1, are placed as grid-forming units, and the ESSs are placed as grid-feeding units, with powers fixed at 50 kW. Table 2 lists the detailed grid model parameters. In validating

the effectiveness of the proposed control, the droop controller controls the frequency until it is close to the reference values, and the system is switched to SIFC or the proposed FRCC at 30 s. Fig. 13 illustrates the sudden load changes scenario, where the frequency reference of each generator is denoted as ω^*, the subscript 'SI1' represents Generator 1 under SIFC, and 'FR2' represents Generator 2 under FRCC. The graph of SIFC is presented as a dashed line, whereas that of FRCC is represented by a solid line.

A. SUDDEN LOAD DISTURBANCES

The load abruptly increased by 50 kW at 1 00 s and decreased by 30 kW at 150 s. Fig. 13(a) and Fig. 13(b) demonstrated that the proposed FRCC could control the active power in the steady state without clock drift, whereas ω_{sys} converged to ω_0. However, in this scenario, the conventional SIFC could not converge the active power of each generator. Similarly, as shown in Fig. 13(c), the frequency restoration term $\delta\omega_{SI1}$ gradually increased, and $\delta\omega_{SI2}$ decreased while $\delta\omega_{FR1}$ and $\delta\omega_{FR2}$ reached a steady state.

B. PLUG-AND-PLAY

As shown in Fig. 14, similar to Fig. 13, the transition from primary droop control to conventional SIFC and FRCC occurred at 30 s, and the load abruptly increased by 50 kW at 100 s. Subsequently, Generator 3 was plugged into the grid near load 2, as shown in Fig. 7 at 150 s. The plugged-in generator has the same specifications as Generator 1 and operated only as the primary frequency droop control until it reached a set point. Subsequently, it switched to either SIFC or FRCC by itself. Even with the addition of new generators to the microgrid, the proposed FRCC method effectively controlled the frequency without clock drift, whereas the conventional SIFC caused clock drift.

C. FRCC WITH BESS

The coordination between the diesel generator and power converter system is promising for islanded microgrid applications. Therefore, demonstrating the applicability of the proposed FRCC to power converter systems in battery energy storage system (BESS) is crucial. Thus, the conventional SIFC and proposed FRCC with BESS were compared, as shown in Fig. 15. One ESS was set as a grid-forming inverter with the proposed FRCC, whereas the other ESS was set as a grid-feeding inverter. The uppercase 'SI' and 'FR' in the notation denote the SIFC and FRCC, respectively, and the lowercase 'DG' and 'ESS' denote the diesel generator and BESS, respectively.

In the simulation, the generators switched to SIFC or FRCC from the primary frequency droop control at 30 s, and the active load abruptly increased by 50 kW and decreased by 30 kW at 100 s and 150 s, respectively. These conditions are the same as that in the sudden load disturbances scenario but include BESS as the FRCC. The results demonstrated that the SIFC method caused clock drift; that is, the active powers of the DG and BESS gradually increased or decreased.

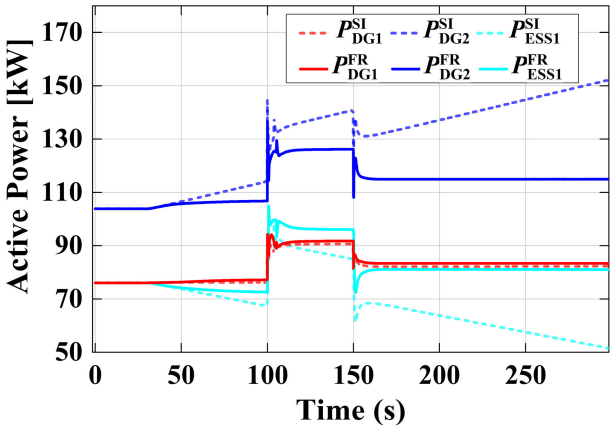

FIGURE 15. Active power of the two diesel generators and one BESS with the proposed FRCC method.

By contrast, the proposed FRCC method did not cause clock drift, and the active power of each generator converged to a steady state. Therefore, BESS can also be adopted as an FRCC method.

VII. CONCLUSION

With conventional secondary frequency controllers, unknown errors in the system or measurement devices can cause clock drift of the controllers or steady-state frequency errors during the parallel operation of diesel generators. Here, we introduce a novel SFC method with compensation signals to mitigate clock drift and eliminate steady-state frequency errors in a decentralized manner without telecommunications. The stability and feasibility of the proposed method were verified using a small-signal state-space model. The proposed method shifted the unstable eigenvalue at the critical point to the negative real part, such that the system matrix was asymptotically stable. Furthermore, CHIL tests and software simulations were performed to demonstrate the effectiveness of the proposed control method. The results confirmed that with the proposed controller, diesel generators could maintain the frequency at a nominal value without telecommunication infrastructure or clock drift. The proposed method can significantly enhance the system reliability of islanded microgrids with a simple implementation.

APPENDIX

The detailed small-signal state-space model of the two generators in (14) can be derived as shown at the top of the next page, where a_1, a_2, a_3, and a_4 are the inner coefficients of $\mathbf{A}_{xk}$. In addition, $\mathbf{B}_{gen}$ can be divided into $\mathbf{B}_{load}$ and $\mathbf{B}_d$, which are input matrices representing the load disturbance and unknown biased errors, respectively. $\mathbf{A}_{pk}$ represents the influence of the active power from each generator on the system frequency, $\mathbf{A}_{\omega k}$ represents the influence of the system frequency on the active power of each generator, $\mathbf{A}_{xk}$ represents the primary and secondary frequency control of

$$
\begin{aligned}
\mathbf{A}_{\text{gen}} &= \begin{bmatrix} -D/M_{eq} & \mathbf{A}_{p1} & \mathbf{A}_{p2} \\ \mathbf{A}_{\omega 1} & \mathbf{A}_{x1} & \mathbf{A}_{y1} \\ \mathbf{A}_{\omega 2} & \mathbf{A}_{y2} & \mathbf{A}_{x2} \end{bmatrix}, \mathbf{B}_{\text{gen}} = \begin{bmatrix} \mathbf{B}_{\text{load}} & \mathbf{B}_d \end{bmatrix}, \\
\mathbf{A}_{pk} &= \begin{bmatrix} 0 & S_{\text{rate}k}/M_{eq} & 0 & 0 \end{bmatrix}, \\
\mathbf{A}_{\omega k} &= \begin{bmatrix} \mathbf{O}_{1\times 3} & (-k_{1i} + Dk_{1p}/M_{eq})T_{mk} \end{bmatrix}^T, \\
\mathbf{A}_{xk} &= \begin{bmatrix} -m_k k_{i2} & -m_k & 0 & 0 \\ 0 & 0 & 1 & 0 \\ 0 & 0 & 0 & 1 \\ a_1 & a_2 & a_3 & a_4 \end{bmatrix}, \mathbf{A}_{yk} = \begin{bmatrix} \mathbf{O}_{1\times 3} \\ -k_{1p}T_{mk}\mathbf{A}_{pk} \end{bmatrix}, \\
\mathbf{B}_{\text{load}} &= \begin{bmatrix} -1/M_{eq} & \mathbf{O}_{1\times 3} & k_{1p}S_{\text{rate}1}T_{m1}/M_{eq} & \mathbf{O}_{1\times 3} & k_{1p}S_{\text{rate}2}T_{m2}/M_{eq} \end{bmatrix}^T, \\
\mathbf{B}_d &= \begin{bmatrix} \mathbf{B}_{d1} & \mathbf{B}_{d2} \end{bmatrix}, \mathbf{B}_{d1} = \begin{bmatrix} 0 & \mathbf{O}_{1\times 3} & -k_{1i}T_{m1} & \mathbf{O}_{1\times 3} & 0 \end{bmatrix}^T, \\
\mathbf{B}_{d2} &= \begin{bmatrix} 0 & \mathbf{O}_{1\times 3} & 0 & \mathbf{O}_{1\times 3} & -k_{1i}T_{m2} \end{bmatrix}^T, a_1 = (k_{1i} - m_k k_{1p} k_{i2})T_{mk}, a_2 = -k_{1p}S_{\text{rate}k}T_{mk}/M_{eq}, \\
a_3 &= (-1 - m_k k_{1p})T_{mk}, a_4 = -(T_{vk} + T_{ek})T_{mk}, \\
M_{eq} &= M_1 + M_2,
\end{aligned}
$$

each generator, and $\mathbf{A}_{\mathbf{y}k}$ represents the influence of the active power of the other generators to each generator.

REFERENCES

[1] D. E. Olivares, A. Mehrizi-Sani, A. H. Etemadi, C. A. Cañizares, R. Iravani, M. Kazerani, A. H. Hajimiragha, O. Gomis-Bellmunt, M. Saeedifard, R. Palma-Behnke, G. A. Jiménez-Estévez, and N. D. Hatziargyriou, "Trends in microgrid control," *IEEE Trans. Smart Grid*, vol. 5, no. 4, pp. 1905–1919, Jul. 2014.

[2] A. Bidram and A. Davoudi, "Hierarchical structure of microgrids control system," *IEEE Trans. Smart Grid*, vol. 3, no. 4, pp. 1963–1976, Dec. 2012.

[3] M. Beus, F. Banis, H. Pandžić, and N. K. Poulsen, "Three-level hierarchical microgrid control—Model development and laboratory implementation," *Electric Power Syst. Res.*, vol. 189, Dec. 2020, Art. no. 106758.

[4] T. L. Vandoorn, B. Renders, L. Degroote, B. Meersman, and L. Vandevelde, "Active load control in islanded microgrids based on the grid voltage," *IEEE Trans. Smart Grid*, vol. 2, no. 1, pp. 139–151, Mar. 2011.

[5] A. Kahrobaeian and Y. A. Ibrahim Mohamed, "Networked-based hybrid distributed power sharing and control for islanded microgrid systems," *IEEE Trans. Power Electron.*, vol. 30, no. 2, pp. 603–617, Feb. 2015.

[6] C. Sun, G. Joos, S. Q. Ali, J. N. Paquin, C. M. Rangel, F. A. Jajeh, I. Novickij, and F. Bouffard, "Design and real-time implementation of a centralized microgrid control system with rule-based dispatch and seamless transition function," *IEEE Trans. Ind. Appl.*, vol. 56, no. 3, pp. 3168–3177, May 2020.

[7] N. L. Díaz, A. C. Luna, J. C. Vasquez, and J. M. Guerrero, "Centralized control architecture for coordination of distributed renewable generation and energy storage in islanded AC microgrids," *IEEE Trans. Power Electron.*, vol. 32, no. 7, pp. 5202–5213, Jul. 2017.

[8] A. Bani-Ahmed, M. Rashidi, A. Nasiri, and H. Hosseini, "Reliability analysis of a decentralized microgrid control architecture," *IEEE Trans. Smart Grid*, vol. 10, no. 4, pp. 3910–3918, Jul. 2019.

[9] A. Bani-Ahmed, A. Nasiri, and H. Hosseini, "Design and development of a true decentralized control architecture for microgrid," in *Proc. IEEE Energy Convers. Congr. Expo. (ECCE)*, Sep. 2016, pp. 1–5.

[10] T. Dragicevic, R. Heydari, and F. Blaabjerg, "Super-high bandwidth secondary control of AC microgrids," in *Proc. IEEE Appl. Power Electron. Conf. Expo. (APEC)*, Mar. 2018, pp. 3036–3042.

[11] R. Heydari, T. Dragicevic, and F. Blaabjerg, "High-bandwidth secondary voltage and frequency control of VSC-based AC microgrid," *IEEE Trans. Power Electron.*, vol. 34, no. 11, pp. 11320–11331, Nov. 2019.

[12] C. Peng, H. Sun, M. Yang, and Y.-L. Wang, "A survey on security communication and control for smart grids under malicious cyber attacks," *IEEE Trans. Syst. Man, Cybern. Syst.*, vol. 49, no. 8, pp. 1554–1569, Aug. 2019.

[13] J. W. Simpson-Porco, Q. Shafiee, F. Dörfler, J. C. Vasquez, J. M. Guerrero, and F. Bullo, "Secondary frequency and voltage control of islanded microgrids via distributed averaging," *IEEE Trans. Ind. Electron.*, vol. 62, no. 11, pp. 7025–7038, Nov. 2015.

[14] M. Chen, X. Xiao, and J. M. Guerrero, "Secondary restoration control of islanded microgrids with a decentralized event-triggered strategy," *IEEE Trans. Ind. Informat.*, vol. 14, no. 9, pp. 3870–3880, Sep. 2018.

[15] W. W. A. G. da Silva, T. R. Oliveira, and P. F. Donoso-Garcia, "Hybrid distributed and decentralized secondary control strategy to attain accurate power sharing and improved voltage restoration in DC microgrids," *IEEE Trans. Power Electron.*, vol. 35, no. 6, pp. 6458–6469, Jun. 2020.

[16] Y. Zhang and T. Yang, "Decentralized switching control strategy for load frequency control in multi-area power systems with time delay and packet losses," *IEEE Access*, vol. 8, pp. 15838–15850, 2020.

[17] X. Chen, S. Hu, Y. Li, D. Yue, C. Dou, and L. Ding, "Co-estimation of state and FDI attacks and attack compensation control for multi-area load frequency control systems under FDI and DoS attacks," *IEEE Trans. Smart Grid*, vol. 13, no. 3, pp. 2357–2368, May 2022.

[18] M. Jamali, H. R. Baghaee, M. S. Sadabadi, G. B. Gharehpetian, and A. Anvari-Moghaddam, "Distributed cooperative event-triggered control of cyber-physical AC microgrids subject to denial-of-service attacks," *IEEE Trans. Smart Grid*, vol. 14, no. 6, pp. 4467–4478, Nov. 2023.

[19] S. Feng and P. Tesi, "Resilient control under denial-of-service: Robust design," *Automatica*, vol. 79, pp. 42–51, May 2017.

[20] J. Yang, Q. Zhong, K. Shi, and S. Zhong, "Distributed coordination LFC approach for interconnected power systems under detection and compensation mechanism targeting DoS attacks," *IEEE Trans. Ind. Informat.*, vol. 19, no. 11, pp. 1–10, Nov. 2023.

[21] S. Du, H. Sheng, D. W. C. Ho, and J. Qiao, "Secure consensus of multiagent systems with DoS attacks via fully distributed dynamic event-triggered control," *IEEE Trans. Syst. Man, Cybern. Syst.*, vol. 53, no. 10, pp. 1–10, Oct. 2023.

[22] A.-Y. Lu and G.-H. Yang, "Distributed consensus control for multi-agent systems under denial-of-service," *Inf. Sci.*, vols. 439–440, pp. 95–107, May 2018.

[23] W. Alghamdi and M. Schukat, "Precision time protocol attack strategies and their resistance to existing security extensions," *Cybersecurity*, vol. 4, no. 1, p. 12, Dec. 2021.

[24] S. Ismail, H. R. Hassen, M. Just, and H. Zantout, "A review of amplification-based distributed denial of service attacks and their mitigation," *Comput. Secur.*, vol. 109, Oct. 2021, Art. no. 102380.

[25] Y. Khayat, M. Naderi, Q. Shafiee, Y. Batmani, M. Fathi, J. M. Guerrero, and H. Bevrani, "Decentralized optimal frequency control in autonomous microgrids," *IEEE Trans. Power Syst.*, vol. 34, no. 3, pp. 2345–2353, May 2019.

[26] M. Kosari and S. Hossein Hosseinian, "Decentralized reactive power sharing and frequency restoration in islanded microgrid," *IEEE Trans. Power Syst.*, vol. 32, no. 4, pp. 2901–2912, Jul. 2017.
[27] R. Heydari, Y. Khayat, M. Naderi, A. Anvari-Moghaddam, T. Dragicevic, and F. Blaabjerg, "A decentralized adaptive control method for frequency regulation and power sharing in autonomous microgrids," in *Proc. IEEE 28th Int. Symp. Ind. Electron. (ISIE)*, Jun. 2019, pp. 2427–2432.
[28] J. Schiffer, R. Ortega, C. A. Hans, and J. Raisch, "Droop-controlled inverter-based microgrids are robust to clock drifts," in *Proc. Amer. Control Conf. (ACC)*, Jul. 2015, pp. 2341–2346.
[29] M. Andreasson, D. V. Dimarogonas, H. Sandberg, and K. H. Johansson, "Distributed control of networked dynamical systems: Static feedback, integral action and consensus," *IEEE Trans. Autom. Control*, vol. 59, no. 7, pp. 1750–1764, Jul. 2014.
[30] E. Weitenberg, Y. Jiang, C. Zhao, E. Mallada, C. De Persis, and F. Dörfler, "Robust decentralized secondary frequency control in power systems: Merits and tradeoffs," *IEEE Trans. Autom. Control*, vol. 64, no. 10, pp. 3967–3982, Oct. 2019.
[31] B. Liu, T. Wu, Z. Liu, and J. Liu, "A small-AC-signal injection-based decentralized secondary frequency control for droop-controlled islanded microgrids," *IEEE Trans. Power Electron.*, vol. 35, no. 11, pp. 11634–11651, Nov. 2020.
[32] N. Kanao, Y. Hayashi, and J. Matsuki, "Analysis of even harmonics generation in an isolated electric power system," *Electr. Eng. Jpn.*, vol. 167, no. 2, pp. 56–63, Apr. 2009.
[33] H.-J. Moon, Y. J. Kim, J. W. Chang, and S.-I. Moon, "Decentralised active power control strategy for real-time power balance in an isolated microgrid with an energy storage system and diesel generators," *Energies*, vol. 12, no. 3, p. 511, Feb. 2019.
[34] P. Kundur, N. J. Balu, and M. G. Lauby, *Power System Stability and Control*. New York, NY, USA: McGraw-Hill, 1994.
[35] B. Yu, "An improved frequency measurement method from the digital PLL structure for single-phase grid-connected PV applications," *Electronics*, vol. 7, no. 8, p. 150, Aug. 2018.
[36] A. J. Roscoe, "Measurement, control and protection of microgrids at low frame rates supporting security of supply," Ph.D. dissertation, Dept. Electron. Elect. Eng., Univ. Strathclyde, Glasgow, U.K., 2009.
[37] U. Tamrakar, D. Shrestha, M. Maharjan, B. Bhattarai, T. Hansen, and R. Tonkoski, "Virtual inertia: Current trends and future directions," *Appl. Sci.*, vol. 7, no. 7, p. 654, Jun. 2017.
[38] J. Machowski, J. W. Bialek, and J. R. Bumby, *Power System Dynamics*, 2nd ed., Hoboken, NJ, USA: Wiley, 2008.
[39] N. Bottrell, M. Prodanovic, and T. C. Green, "Dynamic stability of a microgrid with an active load," *IEEE Trans. Power Electron.*, vol. 28, no. 11, pp. 5107–5119, Nov. 2013.
[40] R. Shorten, K. S. Narendra, and O. Mason, "A result on common quadratic Lyapunov functions," in *Proc. 41st IEEE Conf. Decis. Control*, May 2002, pp. 2780–2785.
[41] K. Ogata, *Modern Control Engineering*, 5th ed., Upper Saddle River, NJ, USA: Prentice-Hall, 2010.
[42] B. Enayati, "Impact of IEEE 1547 standard on smart inverters," in *Proc. IEEE Power Energy Society General Meeting*, Aug. 2020, pp. 1–6.
[43] E. F. Campana, G. Fasano, and A. Pinto, "Dynamic analysis for the selection of parameters and initial population, in particle swarm optimization," *J. Global Optim.*, vol. 48, no. 3, pp. 347–397, Nov. 2010.
[44] J. Bergstra and Y. Bengio, "Random search for hyper-parameter optimization," *J. Mach. Learn. Res.*, vol. 13, pp. 281–305, Feb. 2012.

JUN-HYEOK KIM (Student Member, IEEE) received the B.S. degree in electronic engineering from Handong University, Pohang-si, South Korea, in 2019. He is currently pursuing the Ph.D. degree with the Graduate School of Energy Convergence, Gwangju Institute of Science and Technology (GIST), Gwangju, South Korea. His research interests include distribution network analysis, distribution management systems, microgrid operation and control, and artificial intelligence.

JAE-WON CHANG (Member, IEEE) received the B.S. and Ph.D. degrees in electrical and computer engineering from Seoul National University, Seoul, South Korea, in 2015 and 2021, respectively. From 2021 to 2023, he was a Senior Researcher with Korea Institute of Energy Research (KIER). Since 2023, he has been involved as a Faculty Member with Chung-Ang University, Seoul, South Korea, where he is currently an Assistant Professor. His research interests include the estimation, control, and operation of microgrids, distributed networks, and inverter-based power systems.

YUN-SU KIM (Senior Member, IEEE) received the B.S. and Ph.D. degrees in electrical engineering from Seoul National University, Seoul, South Korea, in 2010 and 2016, respectively. He was with Korea Electrotechnology Research Institute (KERI) as a Senior Researcher, from 2015 to 2017. He joined the Faculty of Gwangju Institute of Science and Technology (GIST), in 2018, where he is currently a Professor with the Graduate School of Energy Convergence. He was the Director of Korean Society for New and Renewable Energy and The Korean Institute of Electrical Engineers. His research interests include distribution networks, distributed energy resources, microgrids, artificial intelligence, and wireless power transfer.